Cross-Linking 3D Assemblies of Nanoparticles into Mechanically Strong Aerogels by Surface-Initiated Free-Radical Polymerization

Sudhir Mulik,[†] Chariklia Sotiriou-Leventis,*[,†] Gitogo Churu,[‡] Hongbing Lu,*[,‡] and Nicholas Leventis*[,†]

Department of Chemistry, Missouri University of Science and Technology (formerly, University of Missouri−Rolla), Rolla, Missouri 65409 and Department of Mechanical and Aerospace Engineering, 218 Engineering North, Oklahoma State University, Stillwater, Oklahoma 74078

Received April 4, 2008. Revised Manuscript Received May 14, 2008

Skeletal nanoparticles of porous low-density materials formally classified as aerogels are cross-linked by surface-initiated polymerization (SIP) using a new surface-confined bidentate free-radical initiator structurally related to azobisisobutyronitrile (AIBN). Methylmethacrylate, styrene, and divinylbenzene are introduced in the mesopores, and upon heating at 70 °C, all mesoporous surfaces throughout the entire skeletal framework are coated conformally with a 10−12 nm thick polymer layer indistinguishable spectroscopically from the respective commercial bulk materials. The amount of polymer incorporated in the structure is controlled by the concentration of the monomer in the mesopores, and albeit an up to a 3-fold increase in bulk density (up to 0.6−0.8 g cm^{-3}) and a decrease in the porosity even down to 40%, the materials remain mesoporous with average pore diameters increasing from 20 nm in the native samples to 41 and 62 nm in PMMA and polystyrene cross-linked samples, respectively. The new materials combine hydrophobicity with vastly improved mechanical properties in terms of strength, modulus, and toughness relative to their native (non-cross-linked) counterparts. The effect of polymer accumulation on the modulus has been also simulated numerically. Being able to use SIP for cross-linking 3D assemblies of nanoparticles comprising the skeletal framework of typical aerogels paves the way for the deconvolution of cross-linking from gelation (a free-radical versus an ionic process, respectively), so that ultimately all gelation and cross-linking reagents can be included together in one pot, leading to great process simplification. The mechanical properties of the new materials render them appropriate for anti-ballistic applications (e.g., armor).

1. Introduction

Aerogels are open-cell mesoporous foams with a large internal void space (up to >99%), which is responsible for some very attractive bulk properties such as low density, low dielectric constant, low thermal conductivity, high surface area, and high acoustic impedance.[1,2] Unfortunately, those desirable properties come at a cost: aerogels are extremely fragile materials and do not survive long in applications where they experience mechanical stresses. Polymer cross-linked aerogels seem to alleviate those problems while they retain the desirable properties of their native (non-cross-linked) counterparts.

Silica aerogels resulting from a base-catalyzed gelation process of tetramethoxysilane (TMOS) consist of a three-dimensional network of nanoparticles. The fragility of those materials is traced to the interparticle necks. Those are formed naturally upon particle coagulation during gelation and become wider by dissolution and reprecipitation of silica during aging.[3] As necks become wider, the mechanical strength of the bulk material increases. This process, however, is self-limiting because dissolution and preferential reprecipitation at the necks cannot go on indefinitely; it will stop as soon as the neck curvature is no longer negative. Inspired by the processes taking place during aging of wet gels, another method by which necks can be reinforced is via postgelation incorporation of interparticle polymeric tethers bridging and covalently connecting the skeletal nanoparticles. The resulting materials have been referred to as polymer cross-linked aerogels.[4] Since the reinforcing polymer is confined on the skeletal framework, cross-linked aerogels preserve the

* Address correspondence to these authors. N.L.: Phone 573-341-4391, e-mail leventis@mst.edu. C.S.-L.: Phone 573-341-4353, e-mail cslevent@mst.edu. H.L.: Phone 405-744-5900, e-mail hongbing.lu@okstate.edu.

[†] Missouri University of Science and Technology.

[‡] Oklahoma State University.

(1) Morris, C. A.; Anderson, M. L.; Stroud, R. M.; Merzbacher, C. I.; Rolison, D. R. *Science* **1999**, *284*, 622–624.

(2) (a) Hüsing, N.; Schubert, U. *Angew. Chem., Int. Ed. Engl.* **1998**, *37*, 22–45. (b) Pierre, A. C.; Pajonk, G. M. *Chem. Rev.* **2002**, *102*, 4243–4265.

(3) Einarsrud, M.-A.; Nilsen, E.; Rigacci, A.; Pajonk, G. M.; Buathier, S.; Valette, D.; Durant, M.; Chevalier, B.; Nitz, P.; Ehrburger-Dolle, F. *J. Non-Cryst. Solids* **2001**, *285*, 1–7.

(4) (a) Leventis, N. *Acc. Chem. Res.* **2007**, *40*, 874–884. (b) Leventis, N.; Sotiriou-Leventis, C.; Zhang, G.; Rawashdeh, A.-M. M. *Nano Lett.* **2002**, *2*, 957–960. (c) Zhang, G.; Rawashdeh, A.-M. M.; Sotiriou-Leventis, C.; Leventis, N. *Polym. Prepr.* **2003**, *44*, 35–36. (d) Bertino, M. F.; Hund, J. F.; Zhang, G.; Sotiriou-Leventis, C.; Tokuhiro, A. T.; Leventis, N. *J. Sol-Gel Sci. Technol.* **2004**, *30*, 43–48. (e) Zhang, G.; Dass, A.; Rawashdeh, A.-M. M.; Thomas, J.; Counsil, J. A.; Sotiriou-Leventis, C.; Fabrizio, E. F.; Ilhan, F.; Vassilaras, P.; Scheiman, D. A.; McCorkle, L.; Palczer, A.; Johnston, J. C.; Meador, M. A. B.; Leventis, N. *J. Non-Cryst. Solids* **2004**, *350*, 152–164. (f) Leventis, N.; Palczer, A.; McCorkle, L.; Zhang, G.; Sotiriou-Leventis, C. *J. Sol-Gel Sci. Technol.* **2005**, *35*, 99–105. (g) Leventis, N.; Vassilaras, P.; Fabrizio, E. F.; Dass, A. *J. Mater. Chem.* **2007**, *17*, 1502–1508.

10.1021/cm800963h CCC: $40.75
Published on Web 07/17/2008

porosity and associated attractive properties of their native counterparts.

Classificationwise, polymer cross-linked aerogels are three-dimensional (3D) core−shell superstructures (as opposed to core−shell single particles), and there are three degrees of freedom in their design: the chemical identity of the framework, the chemical identity of the polymer, and the nanoparticle surface functionality. The latter is seemingly the most versatile parameter because by careful choice of the reactive group on the surface of silica one can incorporate a variety of polymers. This has been demonstrated, for instance, with the amine functionality, which has become the point of attachment for polyurea (via reaction with di-isocyanates),[5–8] epoxy resins (via reaction with epoxides),[9] or even polystyrene (PS) after further surface modification with styrene via a lengthy process that involves reaction of dangling amines with *p*-chloromethylstyrene.[10] Cross-linking with isocyanates and epoxides are "grafting from" approaches,[11] while cross-linking with PS is a "grafting to" free-radical method. "Grafting from" provides the most control over building a shell around a core because it uses the latter as the central point of departure for the polymeric chains. Preparation methods of inorganic core/organic shell nanoparticles by the "grafting from" method span the entire range from layer-by-layer electrostatic assembly of oppositely charged materials[12–16] to atom-transfer radical polymerization.[17] In order to combine "grafting from" with free-radical chemistry, the nanoparticle surface needs to be modified with a free-radical initiator, which will induce a so-called surface-initiated polymerization (SIP) process. In that regard, peroxide[18] and azobisisobutyronitrile (AIBN) derivatives[19–21] have been attached to the surface of silica by ionic interactions, physical adsorption, and covalently.[22–27] In almost all cases the free-radical initiator is monodentate, namely, it is attached to the surface of silica by one side only.

For our purpose, namely, with an eye on the efficient large-scale production of polymer cross-linked aerogels, scale-up should be considered together with chemical process design. From that perspective, surface-initiated free-radical cross-linking chemistry is attractive because its precursors can coexist with the sol−gel precursors, and therefore, in principle, the two processes can be switched on selectively, for example, by heat or light, simplifying the cross-linked aerogel preparation process tremendously. This reasoning is akin to ideas advanced in the early 1990s by Novak in relation to sol−gel materials including interpenetrating polymer networks.[28] However, although Novak recognized both the importance of using free-radical polymerization for process simplification and the importance of binding the polymer on the skeletal backbone for avoiding leaching and homogeneity problems, nevertheless he overlooked the possibility of realizing both of those goals and in addition improving the mechanical properties of the composites via surface-initiated free-radical polymerization.[28] Monodentate free-radical initiators have the disadvantage that upon homolytic cleavage they produce one surface-bound radical and release a second radical in the solution, initiating homogeneous polymerization whose products will have to be removed later, introducing more processing steps.[29] Therefore, in order to stand any chance for one-pot synthesis of cross-linked aerogels, we realized that the free-radical initiator should be bidentate. Thus, here we report the facile synthesis of a bis-triethoxysilane derivative of AIBN (compound **1**), its incorporation on the skeletal nanoparticles of silica wet gels, and the synthesis of mechanically strong polymer cross-linked aerogels by SIP of methylmethacrylate (MMA), styrene, and divinylbenzene (DVB). All new materials have been characterized for their macroscopic, microscopic/morphological, chemical, as well as mechanical properties. It turns out that polystyrene and polymethylmethacrylate cross-linked aerogels are among the strongest in that class of materials, and possible applications in ballistic protection (e.g., armor) are clearly visible.

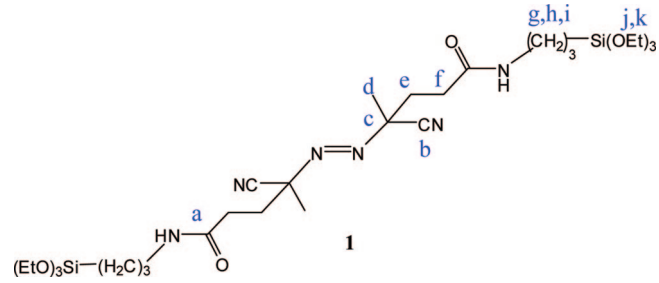

1

2. Experimental Section

2.1. Materials. All reagents and solvents were used as received unless noted otherwise. Azobiscyanovaleric acid (ABCA), ethyl-

(5) Katti, A.; Shimpi, N.; Roy, S.; Lu, H.; Fabrizio, E. F.; Dass, A.; Capadona, L. A.; Leventis, N. *Chem. Mater.* **2006**, *18*, 285–296.
(6) Luo, H.; Lu, H.; Leventis, N. *Mech. Time-Dependent Mater.* **2006**, *10*, 83–111.
(7) Capadona, L. A.; Meador, M. A. B.; Alunni, A.; Fabrizio, E. F.; Vassilaras, P.; Leventis, N. *Polymer* **2006**, *47*, 5754–5761.
(8) Meador, M. A. B.; Capadona, L. A.; McCorkle, L.; Papadopoulos, D. S.; Leventis, N. *Chem. Mater.* **2007**, *19*, 2247–2260.
(9) Meador, M. A. B.; Fabrizio, E. F.; Ilhan, F.; Dass, A.; Zhang, G.; Vassilaras, P.; Johnston, J. C.; Leventis, N. *Chem. Mater.* **2005**, *17*, 1085–1098.
(10) Ilhan, F.; Fabrizio, E. F.; McCorkle, L.; Scheiman, D. A.; Dass, A.; Palczer, A.; Meador, M. A. B.; Johnston, J. C.; Leventis, N. *J. Mater. Chem.* **2006**, *16*, 3046–3054.
(11) Zhao, B.; Brittain, W. J. *Prog. Polym. Sci.* **2000**, *25*, 677–710.
(12) Ou, D. L.; Gould, G. L.; Stepanian, C. J. *U.S. Pat. Appl. Publ. US 2005192366 A1*, 2005.
(13) Keller, S. W.; Johnson, S. A.; Brigham, E. S.; Yonemoto, E. H.; Mallouk, T. E. *J. Am. Chem. Soc.* **1995**, *117*, 12879–12880.
(14) Caruso, F.; Lichtenfeld, H.; Giersig, M.; Möhwald, H. *J. Am. Chem. Soc.* **1998**, *120*, 8523–8524.
(15) Caruso, F.; Caruso, R. A.; Möhwald, H. *Science* **1998**, *282*, 1111–1114.
(16) Caruso, F. *Adv. Mater.* **2001**, *13*, 11–22.
(17) Werne, V.; Patten, T. J. *Am. Chem. Soc.* **2001**, *123*, 7497–7505.
(18) Jiang, W.; Irgum, K. *Anal. Chem.* **2002**, *74*, 4682–4687.
(19) Sulitzky, C.; Rückert, B.; Hall, A. J.; Lanza, F.; Unger, K.; Sellergren, B. *Macromolecules* **2002**, *35*, 79–91.
(20) Fan, X.; Xia, C.; Fulghum, T.; Park, M.-K.; Locklin, J.; Advincula, R. C. *Langmuir* **2003**, *19*, 916–923.
(21) Carlier, E.; Guyot, A.; Revillon, A. *React. Polym.* **1992**, *16*, 115–124.
(22) Fan, X.; Xia, C.; Advincula, R. C. *Langmuir* **2005**, *21*, 2537–2544.
(23) Huang, X.; Brittain, W. J. *Macromolecules* **2001**, *34*, 3255–3260.
(24) Meier, L. P.; Shelden, R. A.; Caseri, W. R.; Suter, U. W. *Macromolecules* **1994**, *27*, 1637–1642.
(25) Prucker, O.; Ruhe, J. *Langmuir* **1998**, *14*, 6893–6898.
(26) Boven, G.; Oosterling, M. L. C. M.; Challa, G.; Schouten, A. J. *Polymer* **1990**, *31*, 2377–2383.
(27) Tsubokawa, N.; Kogure, A.; Maruyama, K.; Sone, Y.; Shimomura, M. *Polym. J.* **1990**, *22* (9), 827–833.

chloroformate, 3-aminopropyltriethoxysilane (APTES), tetramethoxysilane (TMOS), 14.8 N ammonium hydroxide solution, as well as polymethylmethacrylate (PMMA, $M_w \approx 90\,000$; $M_n = 58\,000$) and polystyrene (PS, $M_w \approx 240\,000$; $M_n = 120\,000$), which were used as standards for ^{13}C CMPAS NMR and for differential scanning calorimetry, were purchased from Aldrich Chemical Co. Triethylamine was obtained from Acros Chemicals and further purified by distillation over calcium hydride. Anhydrous tetrahydrofuran (THF) was made by predrying over NaOH and distilling over lithium aluminum hydride. Styrene, methylmethacrylate (MMA), and divinylbenzene (DVB) were purchased from Aldrich Chemical Co. and washed with a 5% (w/w) sodium hydroxide solution in water to remove the inhibitor followed by distillation under reduced pressure. Toluene was purchased from Fisher and purified by stirring overnight with concentrated H_2SO_4 followed by several extractions with water, predrying with Na_2SO_4, followed by a final distillation over phosphorus pentoxide.

Synthesis of 4,4′-(diazene-1,2-diyl)bis-(4-cyano-N-(3-triethoxysilyl)propyl)pentanamide **(1)**. Azobiscyanovaleric acid (ABCA, 30 g, 0.1070 mol) was dissolved in 650 mL of anhydrous THF at room temperature in a jacketed 1 L flask. The solution was maintained under dry and inert conditions (N_2), and the flask was cooled to −76 °C by circulating ethanol using a Neslab's ULT-80 low-temperature bath circulator. After 20 min, ethylchloroformate (20.40 mL, 0.2140 mol) and triethylamine (29.75 mL, 0.2140 mol) were added with a syringe through a septum under magnetic stirring. After another 20 min, APTES (49.93 mL, 0.2140 mol) was added also with a syringe. The reaction temperature was raised to −10 °C, and it was maintained for 24 h. At the end of that period, the reaction mixture was allowed to reach room temperature and filtered under nitrogen in a glovebox. The filtrate was concentrated under reduced pressure followed by addition of hexane. The precipitate was collected in a dry box under nitrogen, recrystallized from THF/hexane twice, and dried under vacuum to give pure product **1** (46.14 g, 63% yield), which was stored as a 0.112 M solution in THF in a refrigerator at 10 °C. ^1H NMR δ 6.05 (2 H, br, s), 3.79 (12 H, q, $J = 7.0$ Hz, $-OCH_2CH_3$), 3.15−3.33 (4 H, m, $-CH_2NH$), 2.13−2.49 (8 H, m, $-CH_2$), 1.67 (6 H, s), 1.56−1.66 (4 H, m, $-CH_2$), 1.20 (18 H, t, $J = 7.0$ Hz, $-CH_2CH_3$), 0.6 (4 H, t, $J = 8.0$ Hz, --CH_2Si). ^{13}C NMR δ 170.1 (C═O), 117.9, 71.8, 58.5, 42.0, 33.9, 31.0, 23.8, 22.7, 18.3, 7.8. IR $\bar{\nu}$ (cm^{-1}) 3430 (m), 2970−2880 (s), 2240 (w), 1640 (s), 1100 (s).

Preparation of Native Silica Aerogels Incorporating **1** *(Native* **Si-1***)*. The stock solution of **1** in THF (0.112 M) was allowed to warm to room temperature, and an aliquot (11.6 mL, 0.0013 mol) was placed in a round-bottom flask. The solvent was removed at room temperature under reduced pressure, and the resulting solid was dissolved in a mixture of 4.5 mL of methanol and 3.465 mL of TMOS (0.0234 mol). This is referred to as Solution A. A second solution (Solution B) was made by mixing 4.5 mL of methanol, 1.5 mL of distilled water, and 40 μL of 14.8 N NH_4OH. Solution B was added into solution A, and the mixture was shaken well and poured into polypropylene molds (Wheaton polypropylene Omni-Vials, Part No. 225402, 1 cm in diameter) or in 19.6 mm diameter, 20 cm^3 polyethylene syringes (samples from the latter were used for compression testing). All solutions gelled within 10−15 min. The resulting wet gels were aged for 24 h at room temperature, solvent-exchanged with acetone (3 washes, 8 h per cycle), and either dried directly in an autoclave to native aerogels with liquid CO_2 taken out supercritically or cross-linked with different olefins as described below.

Preparation of Polymer Cross-Linked Aerogels Incorporating **1** *(***X-Si-1-polymer***)*. For cross-linking, wet-gels incorporating **1** in acetone were solvent-exchanged with toluene (3 washes, 8 h per wash cycle). The volume of toluene used for each wash cycle was 5 times the volume of each gel. Subsequently, toluene-filled wet gels were further washed (3 times, 8 h each time) with different monomer solutions in toluene. Again, the volume of the monomer solution used for each wash cycle was 5 times the volume of each gel. Gels were then heated in the last monomer solution at 70 °C for 12 h followed by washing with fresh toluene (3 times, 8 h each time), and they were dried using SCF CO_2 in an autoclave.

(1) Cross-Linking with Methylmethacrylate (MMA) into **X-Si-1-PMMA**: Gels were cross-linked with 10%, 25%, 30%, 40%, and 50% v/v solutions of MMA in toluene.

(2) Cross-Linking with Styrene into **X-Si-1-PS**: In addition to pure styrene, gels were also cross-linked with several different concentrations of styrene in toluene (10%, 25%, 50%, 75%, and 100% v/v).

(3) Cross-Linking with Divinylbenzene (DVB) into **X-Si-1-PDVB**: Gels were cross-linked with 10%, 25% and 50% v/v solutions of DVB in toluene.

2.2. Methods. Supercritical fluid CO_2 drying was conducted using an autoclave (SPI-DRY Jumbo Supercritical Point Drier, SPI Supplies, Inc., West Chester, PA). Bulk densities (ρ_b) were calculated from the weight and the physical dimensions of the samples. Skeletal densities (ρ_s) were determined using helium pycnometry with a Micromeritics AcuuPyc II 1340 instrument. Porosities were determined from ρ_b and ρ_s. Porosities of selected cross-linked samples were also determined gravimetrically by dipping them in methylcyclohexane followed by weighing and determination of the amount of cyclohexane uptaken. Mesoporous surface areas (σ) and pore size distributions were measured by nitrogen adsorption/desorption porosimetry using a Quantachrome Autosorb-1 Surface Area/Pore Distribution analyzer. Samples for surface area and skeletal density determination were outgassed for 24 h at 80 °C under vacuum before analysis. Average pore diameters were determined by the $4 \times V_{Total}/\sigma$ method, where V_{Total} is the total pore volume per gram of sample. V_{Total} can be calculated either from the single highest volume of N_2 adsorbed along the adsorption isotherm or from the relationship $V_{Total} = (1/\rho_b) - (1/\rho_s)$. The single-point N_2 adsorption method tends to underestimate V_{Total} significantly when macropores are involved.[30] Table 1 cites average pore diameter values by both methods, and the values agree well except when macropores are involved (the presence of the latter was confirmed by SEM). The discussion of average pore diameters is based on values calculated using $V_{Total} = (1/\rho_b) - (1/\rho_s)$. The liquid ^{13}C NMR of compound **1** was recorded using a 400 MHz Varian Unity Inova NMR instrument. Chemical characterization of native and cross-linked silica aerogels was conducted with infrared and solid-state ^{13}C and ^{29}Si NMR spectroscopy. Infrared spectra were obtained in KBr pellets using a Nicolet-FTIR model 750 Spectrometer. Solid ^{13}C NMR spectra were obtained with samples ground in fine powders on a Bruker Avance 300 Spectrometer with 75.475 MHz carbon frequency using magic angle spinning (at 7 kHz) with broadband proton suppression and the CPMAS TOSS pulse sequence for spin sideband suppression. ^{13}C NMR spectra were externally referenced to the carbonyl of glycine (196.1 ppm relative to tetramethylsilane). Thermogravimetric analysis (TGA) was conducted with a TA Instrument, model Hi-Res-TGA 2950, under air and with a heating rate of 10 °C min^{-1}. Modulated

(28) Ellsworth, M. W.; Novak, B. M. *J. Am. Chem. Soc.* **1991**, *113*, 2756–2758. (b) Novak, B. M.; Davies, C. *Macromolecules* **1991**, *24*, 5481–5483. (c) Ellsworth, M. W.; Novak, B. M. *Chem. Mater.* **1993**, *5*, 839–844. (d) Novak, B. M.; Auerbach, D.; Verrier, C. *Chem. Mater.* **1994**, *6*, 282–286.

(29) Prucker, O.; Ruhe, J. *Macromolecules* **1998**, *31*, 592–601.

(30) Fricke, J.; Reichenauer, G. *J. Non-Cryst. Solids* **1987**, *95&96*, 1135–1142.

Table 1. Selected Properties of X-Si-1-polymer (polymer: PMMA, PS, or PDVB)

material	diameter(cm)	bulk density, ρ_b (g cm^{-3})	skeletal density, ρ_s (g cm^{-3})	porosity, Π (% void space)	BET surface area, σ [average pore diameter] [a] (m^2g^{-1}[nm])	force at failure [b] (N)	failure stress [b] (MPa)	flexural modulus, E [b] (MPa)	total % mass loss (by TGA)	% polymer (eq 2)
native silica	0.999 ± 0.002	0.169 ± 0.004	1.981 ± 0.017	92	997 [13.4; 21.7]	[c]	[c]	[c]	4	[d]
native **Si-1**	0.910 ± 0.005	0.189 ± 0.005	1.8516 ± 0.008	90	973 [22.9; 19.5]	[c]	[c]	[c]	21	[d]
X-Si-1-PMMA from 50% MMA	0.885 ± 0.032	0.807 ± 0.047	1.304 ± 0.001	38 (39)[c]	46.05 [31.1; 41.0]	1057.65 ± 54.15	93.13 ± 5.29	618.54 ± 79.31	77	74
X-Si-1-PMMA from 40% MMA	0.928 ± 0.004	0.436 ± 0.036	1.416 ± 0.002	69	185.7 [36.2; 34.2]	272.10 ± 49.95	19.79 ± 3.37	64.59 ± 19.44	62	58
X-Si-1-PMMA from 30% MMA	0.850 ± 0.045	0.261 ± 0.013	1.855 ± 0.008	86	740 [24.7; 17.8]	[c]	[c]	[c]	19	11
X-Si-1-PMMA from 25% MMA	0.968 ± 0.011	0.198 ± 0.028	1.799 ± 0.003	89	787.1 [27.6; 22.8]	[c]	[c]	[c]	45	21
X-Si-1-PMMA from 0% MMA	0.961 ± 0.014	0.174 ± 0.011	1.798 ± 005	90	731.3 [27.7; 28.4]	0.68 ± 0.10	0.05 ± 0.01	1.08 ± 0.11	24	8
X-Si-1-PS from 100% styrene	0.881 ± 0.020	0.549 ± 0.042	1.260 ± 0.001	56 (60)[c]	65.98 [43.7; 62.3]	329.51 ± 32.58	28.86 ± 2.36	192.08 ± 17.98	68	62
X-Si-1-PS from 75% styrene	0.909 ± 0.012	0.333 ± 0.014	1.396 ± 0.002	76	160 [33.5; 57.2]	104.55 ± 14.31	8.10 ± 1.17	27.50 ± 3.92	54	43
X-Si-1-PS from 50% styrene	0.931 ± 0.005	0.325 ± 0.008	1.383 ± 0.002	77	183.4 [43.7; 51.3]	118.55 ± 12.96	8.60 ± 0.94	27.75 ± 2.69	54	46
X-Si-1-PS from 25% styrene	0.925 ± 0.003	0.232 ± 0.016	1.744 ± 0.005	87	620 [27.7; 32.6]	14.90 ± 5.38	1.09 ± 0.39	7.81 ± 0.78	40	22
X-Si-1-PS from 10% styrene	0.963 ± 0.036	0.200 ± 0.031	1.739 ± 0.003	89	668.3 [28.7; 26.5]	1.44 ± 0.41	0.09 ± 0.03	1.30 ± 0.12	24	20
X-Si-1-PDVB from 50% DVB	0.888 ± 0.011	0.795 ± 0.015	1.246 ± 0.001	36	247.0 [5.60; 7.36]	11.90 ± 3.23	0.99 ± 0.31	50.96 ± 18.45	69	74
X-Si-1-PDVB from 25% DVB	0.919 ± 0.005	0.310 ± 0.005	1.437 ± 0.003	78	530.2 [13.7; 19.1]	11.40 ± 1.87	0.85 ± 0.15	17.99 ± 0.86	52	41
X-Si-1-PDVB from 10% DVB	0.986 ± 0.008	0.276 ± 0.002	1.624 ± 0.003	83	731.4 [20.2; 16.4]	n/a	n/a	n/a	34	46

[a] By the $4 \times V_{Total}/\sigma$ method. For the first number, V_{Total} was calculated by the single-point adsorption method; for the second number it was calculated via $V_{Total} = (1/\rho_b) - (1/\rho_s)$. [b] By a short-beam three-point flexural bending method; values are averages of 5 samples. [c] Too weak to measure. [d] Not applicable. [e] Numbers in parentheses determined by the gravimetric cyclohexane rewetting method (see Experimental Section).

differential scanning calorimetry (MDSC) was conducted under nitrogen with a TA Instrument model 2920 apparatus at a heating rate of 10 °C min^{-1}. The mass of each sample was approximately 8−12 mg. Samples were subjected to two heating scans and one cooling scan from 30 to 250 °C. Glass transition temperatures were determined from the second heating scan. Scanning electron microscopy was conducted with samples coated with Au using a Hitachi S-4700 field emission microscope. Three-point flexural bending tests were performed according to ASTM D790, Procedure A (Flexural Properties of Unreinforced and Reinforced Plastics and Electrical Insulating Materials), using an Instron 4469 universal testing machine frame with a 2 kN load cell (Instron part number 2525−818) and a three-point bend fixture with a 22.9 mm span and 25 mm roller diameter (Instron part number 2810−182). Typical samples were cylindrical, ∼1 cm in diameter, and ∼ 4 cm in length. The crosshead speed was set at 1.0 mm min^{-1}.[4b,e] Compression testing was performed according to the ASTM D695-02a standard on cylindrical specimens using a MTS machine (model 810) equipped with a 55 000 lb load cell, as described previously.[5] According to the ASTM standard, the height-to-diameter ratio of the specimen should be 2:1; typical samples were ∼1.5 cm in diameter and 3 cm long.

3. Results and Discussion

3.1. Synthesis, Incorporation of 1 in Mesoporous Silica, and Preparation of Polymer Cross-Linked Aerogels. Typically, skeletal nanoparticles of silica aerogels are provided with functionality by cogelation of tetramethoxy- or tetraethoxysilane (TMOS or TEOS, respectively) with appropriately modified trimethoxy- or triethoxysilanes.[2] In the same context, skeletal nanoparticles of base-catalyzed aerogels are modified with a bidentate free-radical initiator by cogelation of TMOS and **1**. The latter was synthesized in one pot according to Scheme 1 by activation of commercially available azobiscyanovaleric acid (**2**) with ethyl chloroformate (**3**) followed by amidization with 3-aminopropyltriethoxysilane (APTES).[31] Two recrystallizations were necessary for removing acid impurities, which otherwise react and deactivate the base catalyst (NH_4OH) used in the gelation process. Product **1** is sensitive to moisture and tends to self-condense. To prolong its shelf life (up to 2−3 weeks),

Scheme 1. Preparation of the Bidentate Initiator 1

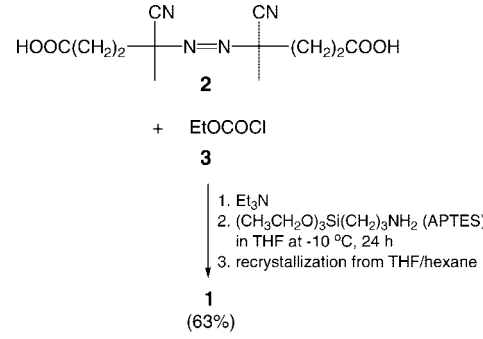

(31) Although the diester analogue of **1** is known,[32] here we decided to work with **1** because its one-pot synthesis is more attractive than the three-step literature method for preparation of its diester analogue.

(32) Parvole, J.; Billon, L.; Montfort, J. P. *Polym. Int.* **2002**, *51*, 1111–1116.

Scheme 2. Preparation of native Silica Aerogels Incorporating 1 (native Si-1) and Cross-Linking with MMA, Styrene, or DVB into X-Si-1-polymer

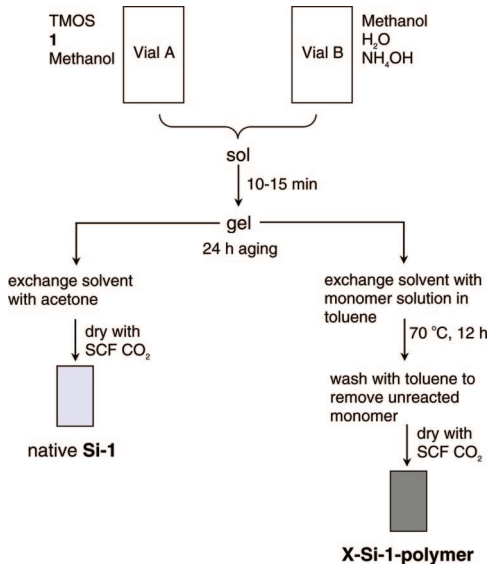

facilitate handling, and standardize processing, **1** was stored as a 0.112 M solution in anhydrous THF at 10 °C.

As with APTES, attempts to induce gelation of **1** by itself were not successful, probably because interference of its side chain with the Si−O−Si network formation. Thus, we resorted to cogelation of **1** with TMOS (Scheme 2). The concentration of **1** was kept low (mol ratio of TMOS:**1** = 18:1) in order to reduce the initiation events and thus obtain cross-linking tethers with higher molecular weight.[33] Under those conditions gelation occurs in 10−15 min, which is not different from gelation of TMOS by itself.[34]

Cross-linking was carried out by first filling the mesopores of the wet gels with various toluene solutions of inhibitor-free monomers (MMA, styrene, or DVB) and subsequently by heating the samples at 70 °C for 12 h (Scheme 2). Unreacted monomer and polymer formed in the mesopores by possible chain-transfer processes were washed off with toluene, and cross-linked monoliths were dried in an autoclave with CO_2 taken out supercritically at the end. Special attention has been paid to internal consistency throughout the process. Polymer cross-linked aerogels are denoted as **X-Si-1-polymer**, where the polymer is either PMMA, PS, or PDVB.

3.2. Physical, Chemical, and Morphological Characterization of Native and Cross-Linked Aerogels. Key properties of all materials reported in this study are summarized in Table 1.

3.2.1. Native Silica Aerogels Incorporating **1.** (native **Si-1**) Although the mole content of **1** in **Si-1** is low (5.6%), the percent weight of **1** in native **Si-1** (assuming complete hydrolysis and condensation of all alkoxyl groups of both TMOS and **1**) is relatively high (30.1% w/w, refer also to the discussion of TGA at the end of this section). Presence

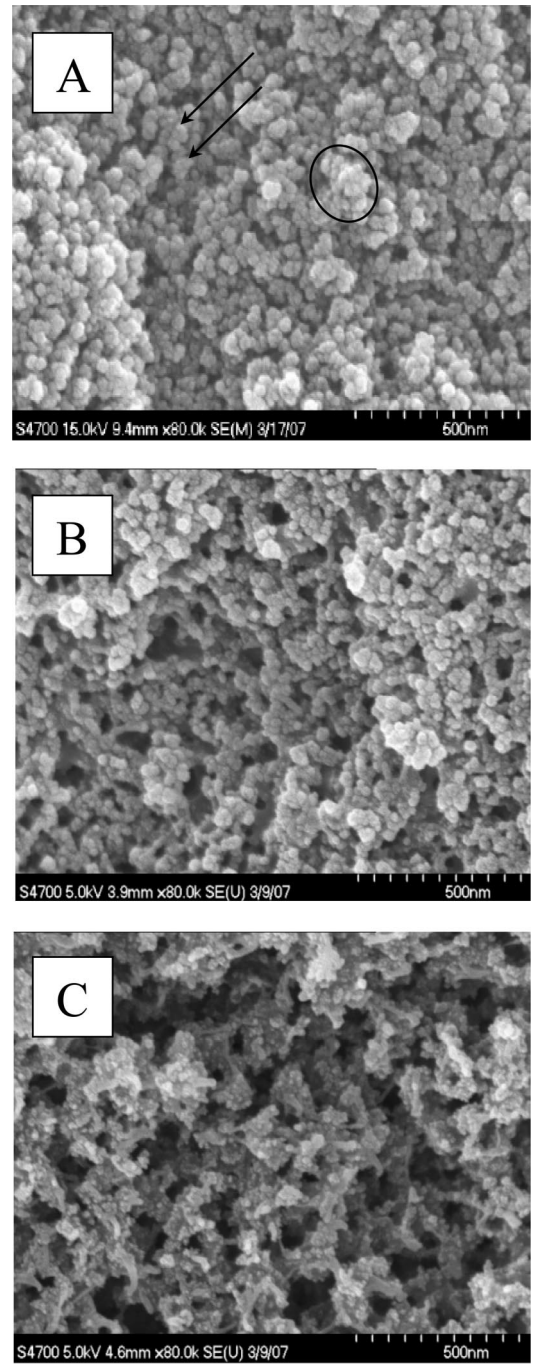

Figure 1. Scanning electron micrographs of (A) native **Si-1** ($\rho_b = 0.189$ g cm^{-3}), (B) **X-Si-1-PMMA** (i.e., **Si-1** cross-linked with PMMA, $\rho_b = 0.807$ g cm^{-3}), and (C) **X-Si-1-PS** (i.e., **Si-1** cross-linked with PS, $\rho_b = 0.549$ g cm^{-3}).

of **1**, however, does not seem to have an adverse effect on the samples in terms of their macroscopic appearance, bulk density, and nanomorphology compared to samples prepared with TMOS only using the same total moles of silica content as in **Si-1**. (Data for such TMOS-only aerogels are also included in Table 1 for comparison.) SEM (Figure 1A) shows that native **Si-1** possesses the characteristic particulate structure of base-catalyzed mesoporous silica, where primary particles are the smallest entities discernible (two are pointed by arrows) and secondary particles consist of larger agglomerations of primary particles (one is shown in a circle). N_2 sorption porosimetry gives type IV isotherms, character-

(33) It is noted that by increasing the concentration of **1** in the sol, the gelation time increases, presumably owing to remaining traces of acid impurities that deactivate the base catalyst.

(34) Leventis, N.; Elder, I. A.; Rolison, D. R.; Anderson, M. L.; Merzbacher, C. I. *Chem. Mater.* **1999**, *11*, 2837–2845.

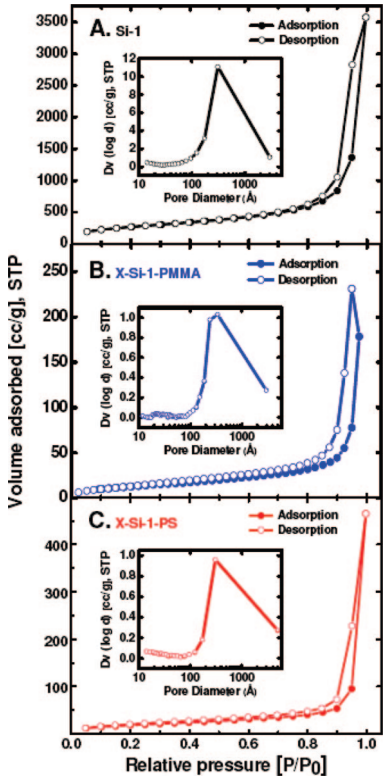

Figure 2. Nitrogen sorption porosimetry. (A) Adsorption−desorption isotherms for a native **Si-1** aerogel ($\rho_b = 0.189$ g cm^{-3}; BET surface area = 973 m^2 g^{-1}; average pore diameter = 29 Å). (B) Adsorption−desorption isotherms for a **X-Si-1-PMMA** aerogel ($\rho_b = 0.807$ g cm^{-3}; BET surface area = 46.1 m^2 g^{-1}; average pore diameter = 39 Å). (C) Adsorption−desorption isotherms for a **X-Si-1-PS** aerogel ($\rho_b = 0.549$ g cm^{-3}; BET surface area = 66.0 m^2 g^{-1}; average pore diameter = 42 Å). (Insets) Pore-size distribution by the BJH method applied on the desorption isotherm.

istic of mesoporous materials (Figure 2A).[35] The BET surface area, σ, is similar to that of TMOS-only samples (~970 m^2 g^{-1}; refer to Table 1).[4a,b] On the basis of the relationship $r = 3/\rho_s\sigma$ (where r = nanoparticle radius and ρ_s = skeletal density of the native **Si-1** aerogels)[36] it is calculated that the nanoparticle diameter is 3.32 nm, corresponding to the primary particles.

The porosity, Π, calculated from bulk and skeletal densities according to eq 1

$$\Pi = \frac{1/\rho_b - 1/\rho_s}{1/\rho_b} \times 100\% \qquad (1)$$

indicates that native **Si-1** aerogels consist of 90% empty space. The average pore diameter is ~20 nm (by the $4 \times V_{Total}/\sigma$ method, where $V_{Total} = (1/\rho_b) - (1/\rho_s)$) and the pore-size distribution at half-width is ~40 nm (Figure 2A, inset). Incorporation of **1** in the skeletal framework is confirmed spectroscopically. Indeed, the infrared (IR) spectrum of **1** is dominated by absorption of the amide C═O stretch at 1640 cm^{-1} and the aliphatic C−H stretches in the 2970−2880 cm^{-1} range (Figure 3). The broad absorption at ~3500 cm^{-1} (O−H stretch) is probably due to some hydrolysis of terminal −Si(OCH$_2$CH$_3$)$_3$ groups, while the weak C≡N stretch

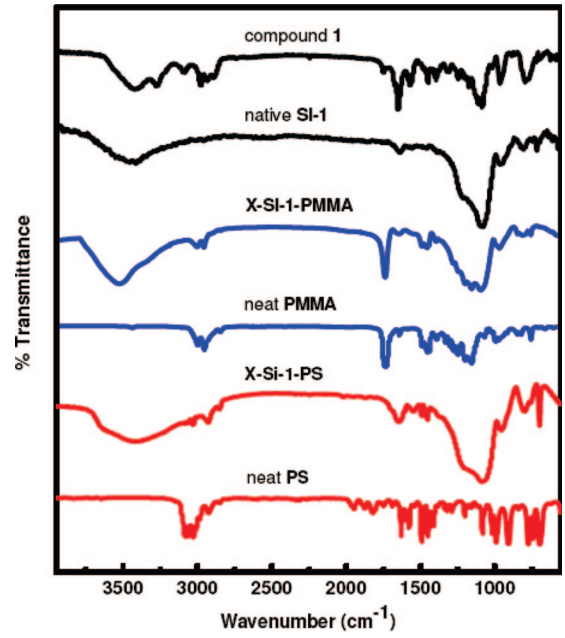

Figure 3. FTIR spectra (in KBr) of compound **1**, native **Si-1**, and cross-linked aerogels **X-Si-1-PMMA** and **X-Si-1-PS** in comparison with neat PMMA and PS.

appears at 2240 cm^{-1}. Now, the IR spectrum of native **Si-1** is dominated by the characteristic Si−O stretch of silica at 1100 cm^{-1} and the broad absorption of surface −OHs in the 3500 cm^{-1} range; the C═O stretch at 1640 cm^{-1} is the only feature of **1** that is still clearly visible in **Si-1**. ^{13}C CPMAS NMR spectra of native **Si-1** aerogels show the carbonyl resonance at 173 ppm and resonances from several aliphatic carbons (Figure 4.) The −CN carbon at 117 ppm is barely visible, while resonances at 16 and 58 ppm (marked with asterisks) correspond to a small amount of unhydrolyzed ethoxy groups from **1**, and the peak at 58 ppm (also marked with an asterisk) corresponds to residual methoxy groups from TMOS. (The sharp peak at 29.2 ppm is likely due to residual solvent, acetone, in the aerogel.) However, the most compelling evidence for incorporation and covalent attachment of **1** comes from ^{29}Si CPMAS NMR (Figure 5). Thus, Figure 5A shows the spectrum of a TMOS-only native silica aerogel: the trimodal resonance between −90 and −110 ppm is assigned to Q^4 (−108 ppm), Q^3 (−99 ppm), and Q^2 (−90.3 ppm) silicon atoms, participating in four, three, and two Si−O−Si bridges, respectively.[37,38] Figure 5B shows that the relative intensity for the Q^2 silicon atoms in **Si-1** aerogels has been reduced, and the new resonances between −50 and −70 ppm are characteristic of T^{3-n} species (n = 0−2), confirming incorporation of **1**.

In principle, **1** could have been partly buried in the interior of the particles. However, based on the fact that hydrolysis of TMOS is expected to be faster than hydrolysis of trialkoxysilanes,[2,36] the probable location of **1** is at the surface of the TMOS-derived nanoparticles. This is consistent with the similar morphology shared by TMOS-only native silica and native **Si-1**. Now, in analogy to AIBN, upon heating, **1**

(35) Sing, K. S. W.; Everett, D. H.; Haul, R. A. W.; Moscou, L.; Pierotti, R. A.; Rouquerol, J.; Siemieniewska, T. *Pure Appl. Chem.* **1985**, *57*, 603–619.
(36) Hüsing, N.; Schubert, U.; Mezei, R.; Fratzl, P.; Riegel, B.; Kiefer, W.; Kohler, D.; Mader, W. *Chem. Mater.* **1999**, *11*, 451–457.
(37) Ek, S.; Iiskola, E. I.; Niinistö, L.; Vaittinen, J.; Pakkanen, T. T.; Root, A. *J. Phys. Chem. B* **2004**, *108*, 11454–11463.
(38) Bonhomme, C.; Coelho, C.; Baccile, N.; Gervais, C.; Azais, T.; Babonneau, F. *Acc. Chem. Res.* **2007**, *40*, 738–746.

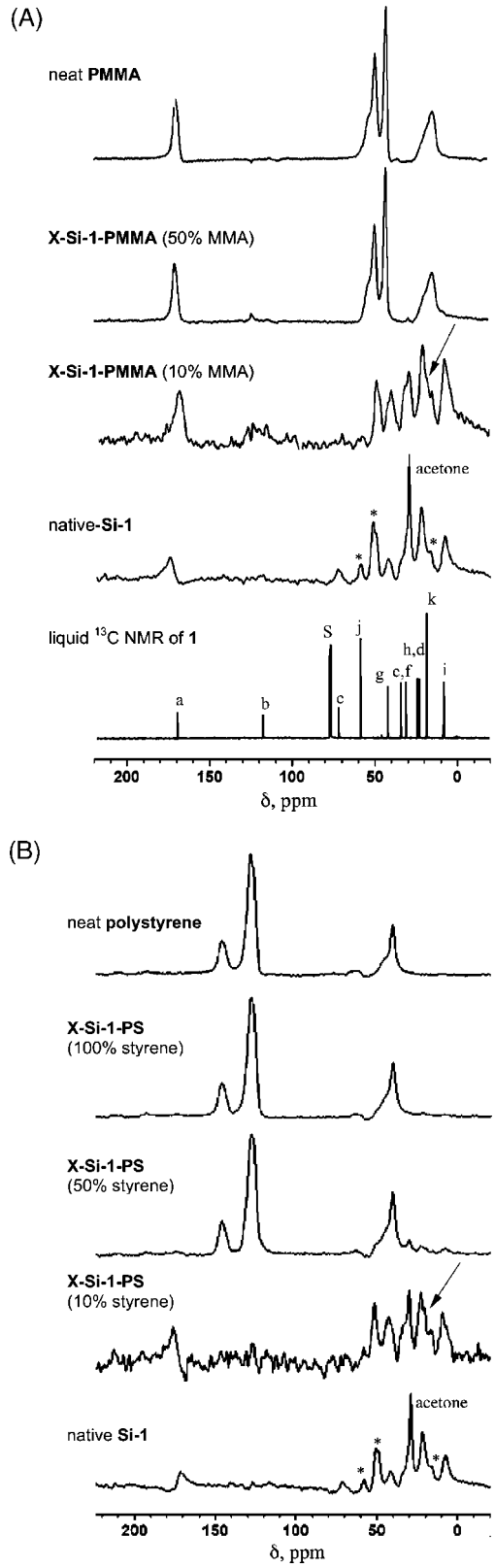

Figure 4. (A) (Bottom) Liquid ^{13}C NMR of **1** in $CDCl_3$ (marked as "S"). For peak assignments, see structure of **1** in the text. (Next four spectra) Solid ^{13}C CPMAS NMR of samples as indicated. The monomer concentrations in the cross-linking bath are shown in parentheses. (B) Solid ^{13}C CPMAS NMR of samples as indicated. The monomer concentrations in the cross-linking bath are shown in parentheses. (Top spectra in both parts) Neat polymers obtained commercially; refer to the Experimental Section. (Peaks marked with asterisks correspond to unhydrolyzed methoxy and ethoxy groups from TMOS and **1**. The shoulder and peak shown by arrows correspond to the radical-bearing carbon of the initiator after it has been attached to the β-carbon of MMA or styrene.)

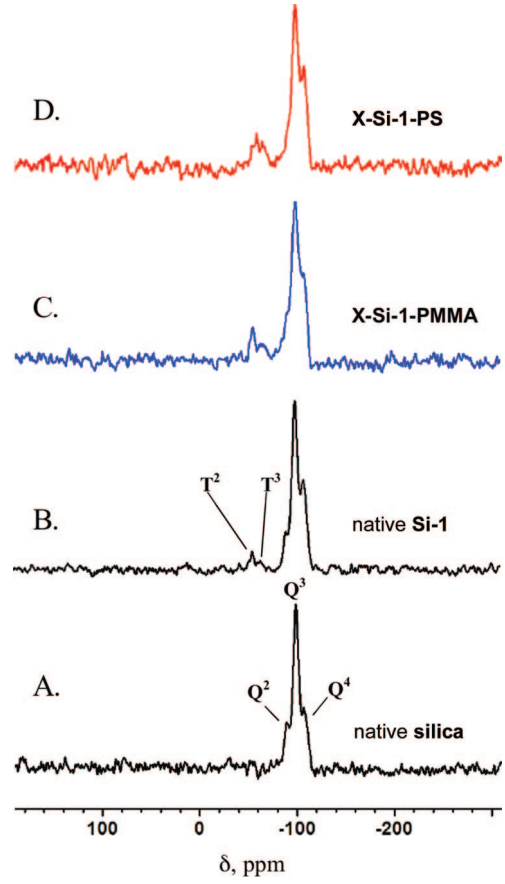

Figure 5. Solid-state ^{29}Si CPMAS NMRs of (A) base-catalyzed, TMOS-only native silica (silica aerogel prepared with the traditional method), (B) native **Si-1** (silica aerogel prepared by cogelation of TMOS and **1**), (C) **X-Si-1-PMMA** (that is **Si-1** cross-linked with PMMA), and (D) **X-Si-1-PS** (that is **Si-1** cross-linked with styrene).

undergoes a sharp mass loss (by TGA, Figure 6A) of ~5% w/w at ~120 °C, attributed to loss of N_2 (versus a theoretical mass loss of 4.08% w/w). The gradual mass loss preceding the sharp decomposition is probably due to residual THF (the storage solvent of **1**) in the sample. Native **Si-1** aerogels also show a TGA step below 120 °C (indicated by an arrow in Figure 6A, inset), which again is assigned to loss of N_2 leaving behind two surface-bound radicals. Finally, in agreement with the expected residual inorganic weight of native **Si-1** (79.8%) calculated assuming complete hydrolysis and condensation of the 18:1 mol ratio of TMOS:**1** in the sol, the overall TGA mass loss of native **Si-1** to 750 °C is 21%.

*3.2.2. Silica Aerogels Cross-Linked with PMMA (***X-Si-1-PMMA***), PS (***X-Si-1-PS***), and PDVB (***X-Si-1-PDVB***).* All monoliths based on **X-Si-1-polymer** are opaque, white, and hydrophobic. Figure 7 shows water droplets on flat surfaces created by cutting cross-linked cylinders vertical to their axes with a diamond saw. The contact angles on **X-Si-1-PMMA** and **X-Si-1-PS** are 72.6 ± 1.3° and 114.1 ± 0.3°, respectively, indicating that the latter material is more hydrophobic than the former, as expected. For comparison, the contact angle of water on PS-cross-linked samples by the "grafing to" method was 121°.[10] Overall, in terms of hydrophobicity, "grafting to" and "grafting from" methods yield similar results; however, for

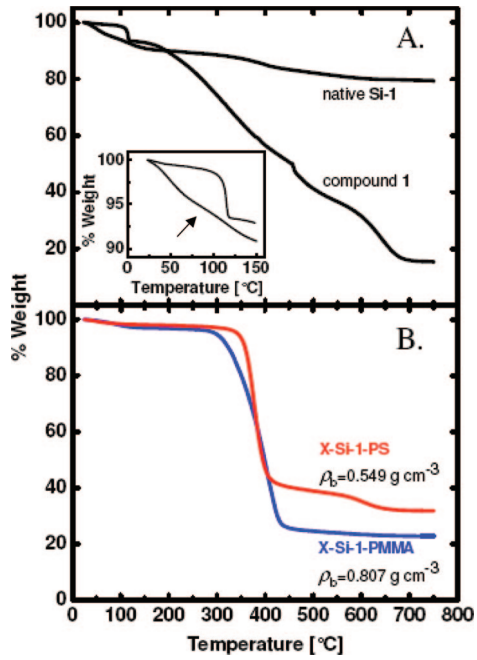

Figure 6. Thermogravimetric analysis (TGA) at 10 °C min^{-1} in air of (A) compound **1** and native **Si-1** and (B) cross-linked samples of **X-Si-1-PMMA** and **X-Si-1-PS** at the densities shown. The total mass loss by **Si-1** (∼20% w/w) correlates well with the 18:1 mol ratio of TMOS:**1** used in the sol (see text). The total mass loss by **X-Si-1-polymer** also correlates well with the amount of polymer calculated by the density increase and monolith size decrease upon cross-linking via eq 3 (see Table 1).

reasons outlined in the Introduction, "grafting from" has certain distinct advantages.

The bulk density (ρ_b) of the three kinds of materials under **X-Si-1-polymer** depends on the chemical identity and concentration of the monomer during incubation. All data have been summarized in Table 1. The amount of polymer uptake is calculated either via the mass loss between 300 and 400 °C in TGA (Figure 6B) or via eq 2, which takes into consideration changes in density and volume after cross-linking.

$$\text{Polymer wt \%} = \left[1 - \left[\left(\frac{\text{diameter}_X}{\text{diameter}_{native}}\right)^3 \left(\frac{\rho_{b,X}}{\rho_{b,native}}\right)\right]^{-1}\right] \times 100 \quad (2)$$

The two methods yield comparable results, although TGA tends to give somewhat higher polymer contents, probably because it does not differentiate between polymer and residual organic material from TMOS and **1** (see discussion of ^{13}C NMR data of native **Si-1** above). At any rate, the polymer content in the most dense samples of all three systems falls in the 60−75% w/w range. Now, it is noted that **X-Si-1-PMMA** samples prepared in 50% v/v MMA/toluene are more dense than **X-Si-1-PS** samples cross-linked in pure styrene. Similary, **X-Si-1-PDVB** cross-linked in 50% v/v DVB are more than twice as dense as **X-Si-1-PS** cross-linked in 50% v/v styrene. These observations are attributed mainly to the higher stability (lower reactivity) of the styrene benzyl radicals.[39] Furthermore, MMA may also develop hydrogen bonding with silanols on the silica surface, creating

(39) Flory, P. J. *Principle of Polymer Chemistry*; Cornell University Press, Limited: 1989; p 195.

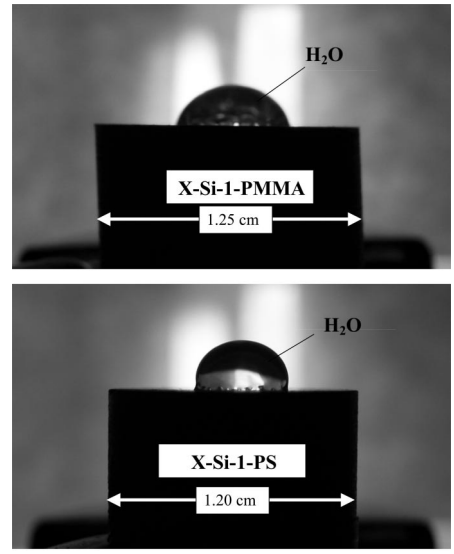

Figure 7. Back-illuminated water droplets on flat surfaces cut off from cylinders of **X-Si-1-PMMA** (ρ_b = 0.66 g cm^{-3}) and **X-Si-1-PS** (ρ_b = 0.48 g cm^{-3}) as indicated. In both cases the materials are hydrophobic and the water droplets are not taken up by the pores, been stable indefinitely.

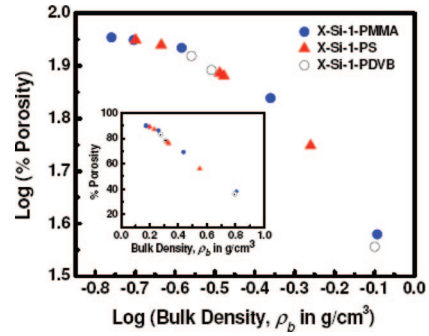

Figure 8. Log(% Porosity) as a function of Log(Bulk Density) for all samples prepared. (Inset) The same quantities plotted on a linear scale. The two quantities correlate with one another independently of the cross-linker, indicating that porosity is a materials property as expected by the design of **X-Si-1-polymer**, whereas the polymer coats the skeletal framework conformally.

a local high concentration of monomer in the vicinity of the initiator, leading to faster accumulation of polymer. Now, for the same cross-linker (MMA, styrene, or DVB), as the monomer concentration increases, the bulk density (ρ_b) of the composite also increases while the skeletal density (ρ_s) decreases. Porosities were again calculated via eq 1, and selected values have been cross-checked gravimetrically by weighing samples before and after dipping in cyclohexane (see Table 1). Porosities by the He pycnometry and cyclohexane uptake methods agree within 3−7% of one another. Porosities correlate with the bulk densities for all three composites independently of the chemical identity of the polymer involved (Figure 8). This is consistent with a material with polymer confined and coating conformally a common skeletal nanostructure. The actual porosity values for the more dense composites are significantly reduced compared to the values of native silica: 36−38% for **X-Si-1-PMMA** (ρ_b = 0.807 g cm^{-3}) and **X-Si-1-PDVB** (ρ_b = 0.795 g cm^{-3}) versus a porosity of 90% for native **Si-1** (ρ_b = 0.189 g cm^{-3}). Despite the apparent reduction in void space, N_2 sorption isotherms remain type IV, indicating that

Scheme 3. Cross-Linking through Termination of Chain Reactions Initiated by a Bidentate Free-Radical Initiator on the Mesoporous Surfaces of 3D Assemblies of Silica Nanoparticles

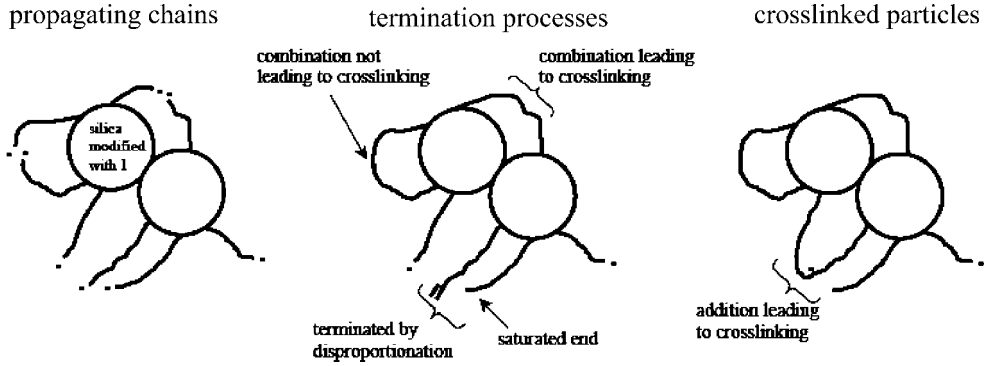

the samples are still mesoporous (Figure 2B and 2C). Nevertheless, the BET surface area has been reduced upon cross-linking from 973 $m^2\ g^{-1}$ for **Si-1** to 46 and 66 $m^2\ g^{-1}$ for **X-Si-1-PMMA** and **X-Si-1-PS** with $\rho_b = 0.807$ g cm^{-3} and 0.549 g cm^{-3}, respectively. At the same time, the average pore diameters of the same samples have been increased relative to native **Si-1** (to 41 and 63 nm for **X-Si-1-PMMA** and **X-Si-1-PS**, respectively, versus 20 nm for **Si-1**). Similarly, the average particle diameter (by the $r = 3/\rho_s\sigma$ method) is 100 and 72 nm for **X-Si-1-PMMA** and **X-Si-1-PS**, respectively (versus an average particle diameter in native **Si-1** before cross-linking of 3.32 nm, which represents the primary particles; refer to section 3.2.a above.) Pore diameters and particle size calculations based on N_2 sorption porosimetry indicate that new material (i.e., polymer) accumulated on the skeletal nanoparticles blocks access of the probe gas (N_2) to the smallest crevices of the native skeletal framework. Thus, in native **Si-1** N_2 sorption samples the primary particles, while in **X-Si-1-PMMA** and **X-Si-1-PS** it samples the secondary ones. Also, another point worth noting is that while the average pore diameter of the **X-Si-1-PMMA** samples is still in the mesoporous range (<50 nm), the average pore diameter of the **X-Si-1-PS** samples is slightly over the upper limit of that range, falling into what is considered macropores. SEM corroborates with this model (Figure 1B and 1C). What is observed is that, first, an open mesoporous structure is still preserved despite the heavy polymer loading. Second, secondary particles are also clearly visible, but in agreement with our previous studies,[4] the fine definition of the primary particles has been erased by the polymer coating. Third, **X-Si-1-PS** samples include macropores. It is speculated that the presence of the latter is the result of the stresses imposed on the skeletal framework by the mechanism of cross-linking, which in turn is related to the free-radical chain termination step (see below).

Spectroscopically, the IR features from silica at 1100 (Si−O stretch) and ~3500 cm^{-1} (O−H stretch) and from PMMA at 1730 (ester C═O stretch) and 3000−2800 cm^{-1} (aliphatic C−H stretch) dominate the spectrum of **X-Si-1-PMMA**, while the amide stretch of the initiator at 1640 cm^{-1} is still visible (Figure 3). Similarly, **X-Si-1-PS** shows the characteristic absorption bands from PS and silica (Figure 3). The ^{29}Si NMR spectra of **X-Si-1-PMMA** (and **-PS**) are practically identical to the spectra of native **Si-1** (Figure 5C and 5D), as expected from the fact that radical formation and cross-linking should not alter the chemical adhesion of the initiator on the surface. On the other hand, ^{13}C CPMAS NMR provides the most direct evidence for involvement of the surface-bound initiator in anchoring the cross-linker (Figure 4). If the monomer concentration in the cross-linking bath (and the mesopores) is kept low (e.g., 10% v/v), the intensity of the polymer peaks remains low, while resonances owing to the surface bound initiator are still clearly visible. Thus, the initiator resonance at 72.27 ppm, which corresponds to the tertiary radical carbon, disappears completely even with small monomer concentrations, while a new resonance at ~19 ppm (pointed at by an arrow) corresponds to the same carbon after it has been added to the β-carbon of MMA or styrene. No new resonances in the aromatic range become evident, signifying no incorporation of toluene through possible chain-transfer processes. At high monomer concentrations, all spectra are dominated by the corresponding polymers, and they are indistiguishable from the spectra of commercially available pure materials (also shown for comparison). At high monomer concentrations, most of the resonances associated with the initiator are either burried underneath the strong resonances of the polymer or remain visible albeit extremely weak (the case of CN in **X-Si-1-PMMA**).

Obviously, polymerization proceeds by addition of surface-bound radicals to monomer from the solution filling the mesopores. Radicals at the tips of polystyrene chains are expected to terminate by combination, bridging particles directly.[40] However, radicals at the tips of propagating PMMA chains will terminate mostly by disproportionation, yielding a saturated group and a new terminal olefin.[40] Addition of a radical at the tip of a neighboring propagating PMMA chain to the newly formed terminal double bond leads to interparticle bridge formation and cross-linking. These processes are summarized in Scheme 3. It is plausible then that chains terminated by combination (case of PS) impose tensile stresses on their nanoparticle pulling the framework apart, creating macropores.

Finally, we have not been able to separate reproducibly the polymers from silica by treating **X-Si-1-polymer** with HF. Therefore, attempts to determine average molecular weights of surface-bound polymers by gel permeation chromatography (GPC) were inconclusive. However, an

(40) (a) Wyzgoski, F. J.; Polce, M. J.; Wesdemiotis, C.; Arnould, M. A. *J. Polym. Sci., Part A: Polym. Chem.* **2007**, *45*, 2161–2171. (b) Buback, M.; Frauendorf, H.; Günzler, F.; Vana, P. *Polymer* **2007**, *48*, 5590–5598.

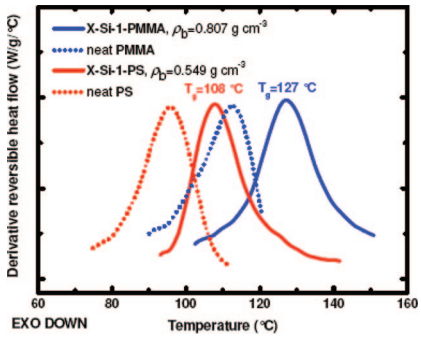

Figure 9. Shift in glass transition temperature (T_g) of PMMA and PS coated conformally and covalently bonded on the skeletal nanoparticles of **X-Si-1-PMMA** and **X-Si-1-PS** in comparison to the neat polymers.

upper and a lower limit for the polymer chain length can be calculated for PS in **X-Si-1-PS** because polymer is expected to be linear and terminated by two molecules of surface-bound initiator. Thus, based on the bulk density of **Si-1** (ρ_b = 0.189 g cm^{-3}) and the 18:1 mol ratio of TMOS:**1** in the sol (or 30.0% w/w of **1** in native **Si-1**), it is first calculated that the skeletal framework contains 1.22 × 10^{-4} mol of initiator/cm^3 of native **Si-1**. Next, the amount (mol) of styrene included in 1 cm^3 of **X-Si-1-PS** can be calculated based on the bulk density increase between native **Si-1** and cross-linked samples (the minor cross-linking shrinkage is ignored). At this point, there are two ways to calculate the number of styrene monomers per polymer chain: either by assuming that all initiator **1** is engaged in initiation events and therefore it finds itself bound at the ends of polymer chains or by assuming that only the fraction of the initiator that is located on the outer surface of the secondary particles is able to create interparticle tethers. An estimate of the latter is obtained from the ratio of the BET surface area after cross-linking over the surface area of native **Si-1**. Thus, it is calculated that PS tethers consist of between 57 and 836 styrene monomer units. Evidently, in comparison with our previous "grafting to" free-radical cross-linking method that yielded PS-cross-linked samples of $\rho_b \approx 0.46$ g cm^{-3} with 15 monomer units of styrene per polymer chain,[10] the present "grafting from" method yields much longer polymers.

Interparticle polymer chains are expected to criss-cross and be stacked on top of one another, but according to SEM the conformal polymer layer should be very thin. Prior experience with this class of materials has shown that TEM is not a reliable tool to differentiate the polymer coating from the silica core.[41,42] On the other hand, we are aware that the restricted mobility of polymeric layers in close proximity to surfaces brings about an increase in their glass transition temperatures (T_g).[43] Indeed (Figure 9), the T_g of PMMA is shifted from 110 °C for the pure isotactic polymer to 127 °C in **X-Si-1-PMMA** (ρ_b = 0.807 g cm^{-3}). Similarly, the T_g of PS is shifted from 95 to 108 °C in **X-Si-1-PS** (ρ_b = 0.549 g cm^{-3}). Those shifts are similar to those reported for polymer brushes made by surface-initiated polymerization of MMA and styrene.[44,45] In particular, according to Yamamoto et al.,[45] an increase of T_g on the order of 17 °C would correspond to a film thickness of ~10−12 nm. In turn, this corresponds to 9−11 layers of fully stretched PMMA with a van der Waals chain diameter of 1.15 nm (by modeling). In fact, that film is what seals access to the space between primary particles, and thus, the average particle size as determined by N_2 sorption data increases from 3.32 nm in native **Si-1** to over 70 nm in **X-Si-1-PMMA** and **X-Si-1-PS**.

3.2.3. Mechanical Properties of **X-Si-1-polymer.** As discussed in the Introduction, practical use of aerogels has been hampered mainly by their fragility. Hydrophilicity also plays a negative role in strength: adsorbed water satisfies the dangling bonds created by Si−O−Si bridge breaking during crack propagation. Aerogels cross-linked with isocyanates and epoxides by the "grafting from" method are mechanically much stronger materials than native aerogels, but they are not hydrophobic.[10] Aerogels cross-linked with polystyrene (and pentafluorostyrene) by the "grafting to" method are hydrophobic but not as strong mechanically as their isocyanate and epoxy counterparts.[10] In order to keep our methodology internally consistent with our previous studies, the mechanical properties of selected aerogel samples cross-linked by the "grafting from" method of this study were tested by two methods: (a) a short-beam three-point flexural bending method and (b) a quasi-static compression testing method, as described in the Experimental Section. In the first method we employed samples of the same dimensions to those used previously for testing isocyanate and epoxy cross-linked samples (i.e., cylinders, ca. 5 cm in length, ca. 1 cm in diameter). As shown in Figure 10A, the most dense samples of **X-Si-1-PMMA** and **X-Si-1-PS** fail with several hundreds Newton, which is comparable to the values we reported for isocyanate and epoxy cross-linked samples of similar densities.[4e,10] For example, **X-Si-1-PMMA** with ρ_b = 0.436 g cm^{-3} fails with 270 N and **X-Si-1-PS** with ρ_b = 0.549 g cm^{-3} fails with 330 N (Table 1). Under the same configuration, isocyanate cross-linked base-catalyzed silica samples of the same geometry having ρ_b = 0.48 g cm^{-3} fail with 190 N,[4e] and "grafting to" PS-cross-linked samples with ρ_b in the range of 0.42−0.48 g cm^{-3} are much weaker, failing with only 42−72 N.[10] Even "grafting to" PS-cross-linked samples with higher bulk densities (ρ_b in the range of 0.6−0.7 g cm^{-3}) still fail more easily with ~150 N.[4e]

From the short-beam bend testing method with cylindrical samples the flexural modulus, E, a measure of stiffness, is calculated via eq 3, and results are cited in Table 1

$$E = \frac{SL^3}{12\pi R^4} \tag{3}$$

where S is the slope of the linear, elastic, part of the load-deformation curve, L is the span, and R is the sample radius.[46]

(41) Leventis, N.; Mulik, S.; Wang, X.; Dass, A.; Sotiriou-Leventis, C.; Lu, H. *J. Am. Chem. Soc.* **2007**, *129*, 10660–10661.
(42) Leventis, N.; Mulik, S.; Wang, X.; Dass, A.; Patil, V.; Sotiriou-Leventis, C.; Lu H.; Churu, G.; Capecelatro, A. *J. Non-Cryst. Solids* **2007,** DOI: 10.1016.
(43) (a) Porter, C. E.; Blum, F. D. *Macromolecules* **2000**, *33*, 7016–7020. (b) Porter, C. E.; Blum, F. D. *Macromolecules* **2002**, *35*, 7448–7452. (c) Metin, B.; Blum, F. D. *J. Chem. Phys.* **2006**, *125*, 054707/1−9.
(44) Vyazovkin, S.; Dranca, I.; Fan, X.; Advincula, R. *J. Phys. Chem. B* **2004**, *108*, 11672–11679.
(45) Yamamoto, S.; Tsujii, Y.; Fukuda, T. *Macromolecules* **2002**, *35*, 6077–6079.

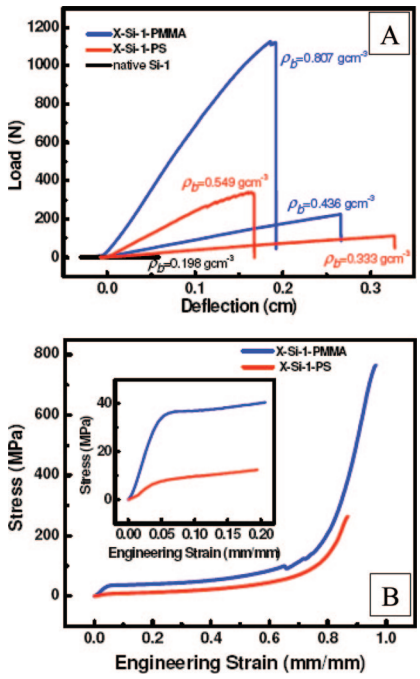

Figure 10. Mechanical characterization of **X-Si-1-PMMA** and **X-Si-1-PS**: (A) by a short-beam three-point flexural testing method and (B) by quasi-static compression.

Scheme 4. Effect of a Conformal Polymer Coating on the Stiffness of a Two-Particle System

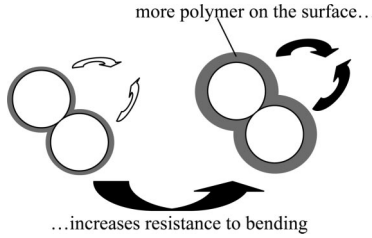

X-Si-1-polymer samples with bulk densities similar to those of samples cross-linked with isocyanates, epoxies, and "grafting to" polystyrene seem to have similar stiffness. This is because increasing the particle diameter of any two-particle system by accumulating material (polymer) on their surface increases their resistance to bending (see Scheme 4 for a qualitative description and the Supporting Information for computer simulations of that effect). In that regard, similar bulk densities correspond to similar amounts of polymer accumulated on the skeletal nanoparticles, increasing resistance to bending by more or less the same amount. On the other hand, the increased strength by the present "grafting from" method versus the polystyrene "grafting to" method is attributed to more effective interparticle tethering (cross-linking).

Under compressive stress (Figure 10B), **X-Si-1-polymer** samples are again decisively stronger than all previously tested isocyanate cross-linked samples that rely on base-catalyzed silica of similar skeletal morphology.[5,6] All stress−strain curves show a linear elastic region at small compressive strains (<6−8%), then exhibit yield behavior (up to ∼50% stain), followed by densification and inelastic hardening (Figure 10B). Samples do not buckle or bend during compression, and the Poisson's ratio remains low (0.18). Figure 11 shows **X-Si-1-PMMA** and **X-Si-1-PS** samples before and after compression; samples turned transparent after compression at 96% strain, signifying a compact material with no voids that would scatter light. Typically, **X-Si-1-PS** with $\rho_b \approx 0.46$ g cm^{-3} show a compressive yield strength (the offset yield strength at 0.2% compressive strain) equal to 7.2 MPa, a compressive stress of 263 MPa at strain 86%, and a Young's modulus, E, of 148 MPa. (By comparison, isocyanate cross-linked samples with $\rho_b \approx 0.48$ g cm^{-3} show a compressive yield strength of 4.3 MPa, a compressive stress of 186 MPa at ∼77% strain, and a Young's modulus of 129 MPa.[5,6]) Remarkably, **X-Si-1-PMMA** samples with $\rho_b \approx 0.66$ g cm^{-3} show a compressive yield strength of 36.1 MPa, a compressive stress of 730 MPa at 96% strain (samples never broke into fragments), and a Young's modulus of 908 MPa. The specific energy absorption of about 194 J g^{-1} surpasses even that of the spider dragline silk (165 J g^{-1}, albeit under tension), which is considered as the toughest natural material.[47] In fact, the mechanical properties of **X-Si-1-PMMA** are in the same "ball park" to those of isocyanate-cross-linked vanadia as well as surfactant-templated, acid-catalyzed sol−gel silica that both possess totally different structural morphologies from what we have seen so far with **X-Si-1-polymer**, consisting of entangled nanoworms rather than nanoparticles.[41,42,48] For instance, one such kind of material (**X-MP4-T045**) with $\rho_b \approx 0.67$ g cm^{-3} shows a compressive yield strength of 15.2 MPa, a compressive stress at failure equal to 804 MPa at 85% strain, and a Young's modulus of 274 MPa, which are values similar to those of **X-Si-1-PMMA** of similar density. The increased strength of cross-linked aerogels consisting of nanoworms rather than nanoparticles has been attributed to a synergistic effect, whereas polymer cross-linking reinforces the contact points (necks) between the nanoworms, which hold the structure together even after several individual contacts between nanoparticles may have been broken. It is plausible that long interparticle polymer chains have a similar effect.

4. Conclusions

Casting a conformal polymer coating on 3D assemblies of sol−gel nanoparticles comprising the skeletal framework of a typical aerogel results in new materials with greatly enhanced mechanical strength. The process is referred to as cross-linking and the materials as cross-linked aerogels. However, so far both the sol−gel and the cross-linking processes have been ionic, and therefore, their reagents could not coexist. Hence, they have been introduced in tandem, adding time-consuming processing steps. In an effort to deconvolute the cross-linking from the gelation process, we synthesized the bidentate free-radical initiator **1** and incorporated it in sol−gel silica. Surface-initiated polymerization (SIP) of MMA, styrene, or DVB by **1** results in conformal

(46) Gere, J. M.; Timoshenko, S. P. *Mechanics of Materials*, 4th ed.; PWS Publishing: Boston, MA, 1997.

(47) Vollrath, F.; Knight, D. P. *Nature* **2001**, *410*, 541–548.

(48) Leventis, N.; Sotiriou-Leventis, C.; Mulik, S.; Dass, A.; Schnobrich, J.; Hobbs, A.; Fabrizio, E. F.; Luo, H.; Churu, G.; Zhang, Y.; Lu, H. *J. Mater. Chem.* **2008**, *18*, 2475–2482.

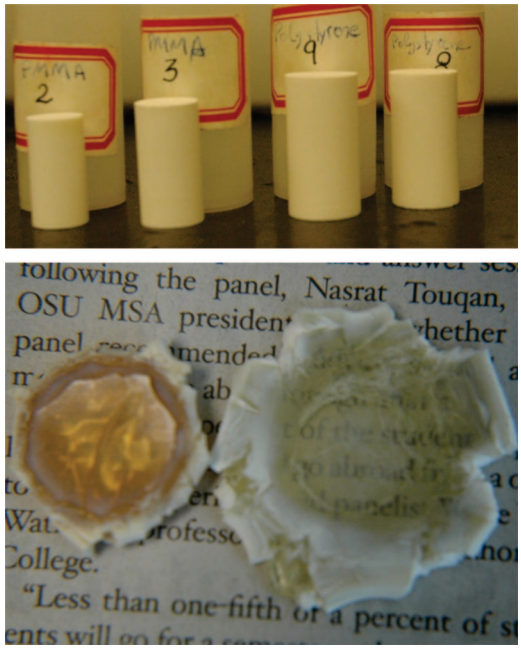

Figure 11. (Top) Samples before compression: (left two) **X-Si-1-PMMA,** $\rho_b = 0.66$ g cm^{-3}; (right two) **X-Si-1-PS**, $\rho_b = 0.46$ g cm^{-3}. (Bottom) Samples after compression: (left) **X-Si-1-PMMA**, compressed by 86% strain; (right) **X-Si-1-PS**, compressed by 96% strain.

polymer coatings on the skeletal nanoparticles, yielding mechanically very strong, hydrophobic materials. A clearly visible application for those new materials is in armor: with a relatively low modulus (e.g., $E = 148$ MPa) and density ($\rho_b = 0.46$ g cm^{-3}), it is calculated that the speed of sound ($c = (E/\rho_b)^{1/2}$) through **X-Si-1-PS** is $c = 635$ m s^{-1}. The latter is very low for a solid material and therefore highly desirable because it will extend the duration of an impact, thereby reducing the effective force on the material. The relatively low yield stress (7.2 MPa for **X-Si-1-PS** with $\rho_b = 0.46$ g cm^{-3}) allows early activation of the energy absorption mechanism, while the long stress plateau allows for large energy absorption. The specific energy absorption at low strain rates that was reported above is 194 J g^{-1}; that value is much higher than that of polymethylacrylamide or Rohacell foams that can achieve specific energy absorptions up to 35 J g^{-1}, which is often considered a high value.[49] Finally, although this research effort has been focused on aerogels, SIP with **1** paves the way for more innovative research at the interface of the sol−gel and polymer chemistry. Examples include improving adhesion of coatings and more efficient preparation of covalently bonded, completely randomized 3D dispersions of nanoparticles as fillers in plastics.

Acknowledgment. We acknowledge the University of Missouri Research Board (N.L.) and the NSF under CMMI-0653919, CHE-0809562 and CMMI-0653970 for financial support. We also thank Dr. Wei Wycoff for her assistance with solids NMR and Professor Douglas K. Ludlow for his assistance with N_2 adsorption porosimetry. We also thank Mr. Nitin P. Daphalapurkar for conducting the finite-element analysis of two connected secondary silica nanoparticles.

Supporting Information Available: Simulation of the bending process of a two-nanoparticle system demonstrating that the Young's modulus of an aerogel monolith increases by accumulation of polymer on the skeletal framework (PDF). This material is available free of charge via the Internet at http://pubs.acs.org.

CM800963H

(49) Gibson, L. J.; Ashby, M. F. *Cellular Solids, Structure and Properties*, 2nd ed.; Cambridge University Press: New York, 1997.